Flux Tube Model Signals in Heavy Ion Collisions

Apoorva Patel

Centre for High Energy Physics and

Supercomputer Education and Research Centre

Indian Institute of Science, Bangalore

18 November 2013, Heavy Ion Forum, CERN

Heavy Ion Collisions

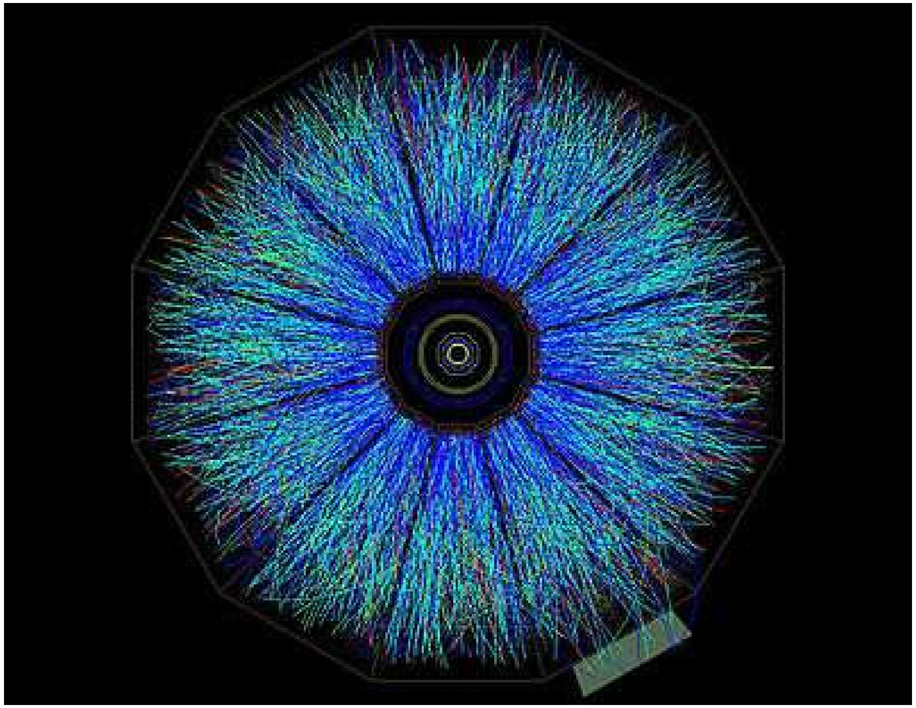

STAR event at RHIC

Au+Au collision at 100+100 GeV/nucleon

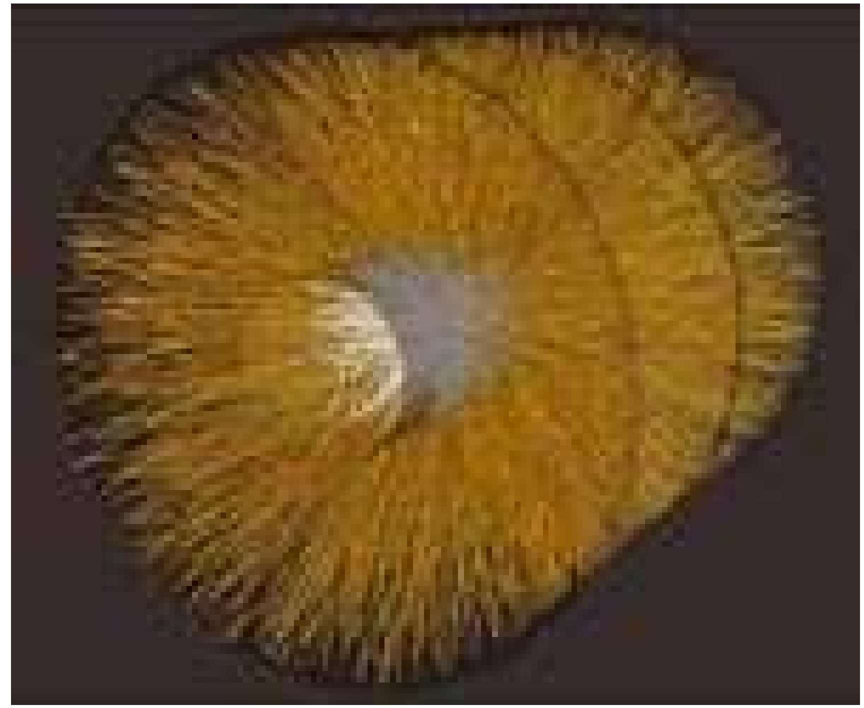

ALICE event at LHC

Pb+Pb collision at 1.38+1.38 TeV/nucleon

Thousands of hadrons are produced.
Only charged ones are detected.

Angular distributions can be meaningfully measured.
Transverse coverage: $\theta_m < \theta < \pi - \theta_m$

CMBR Observations

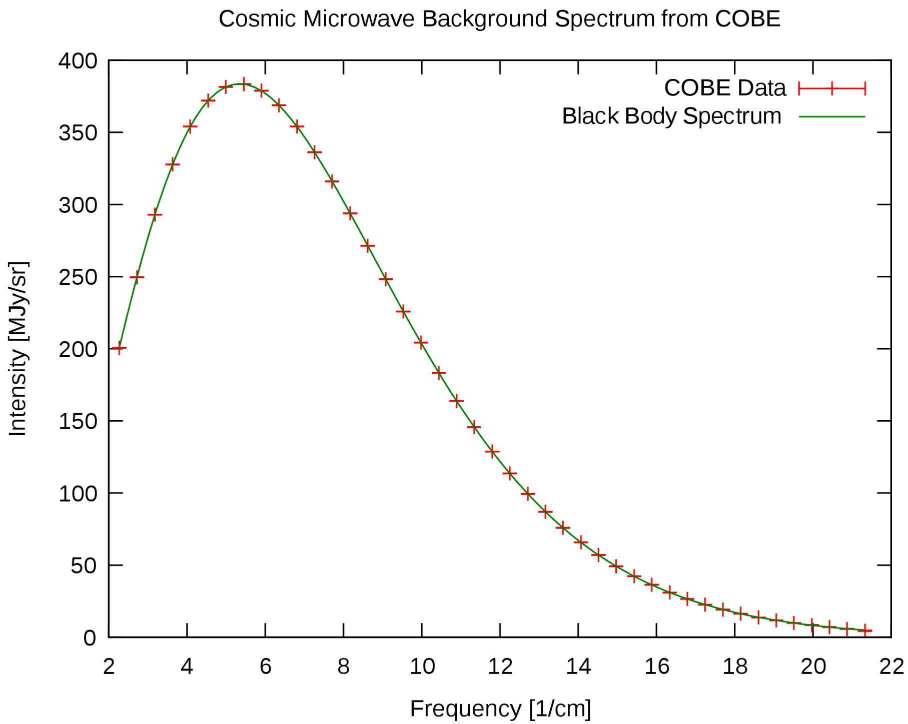

The most precisely measured black body spectrum in nature $T = 2.72548(57)\ {}^\circ K$

CMBR Observations

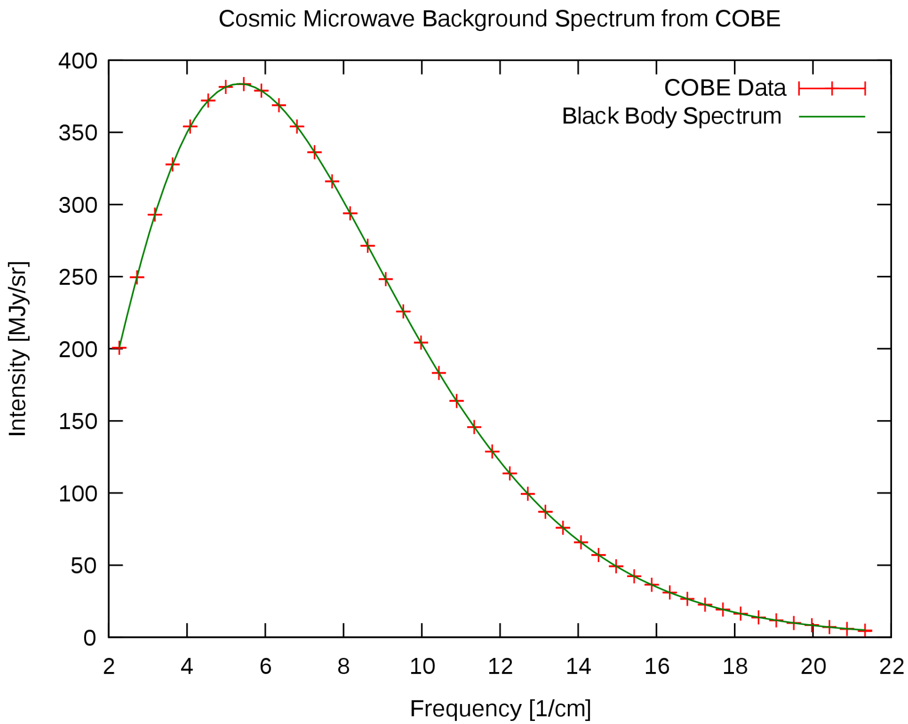

The most precisely measured black body spectrum in nature $T = 2.72548(57)\ ^\circ K$

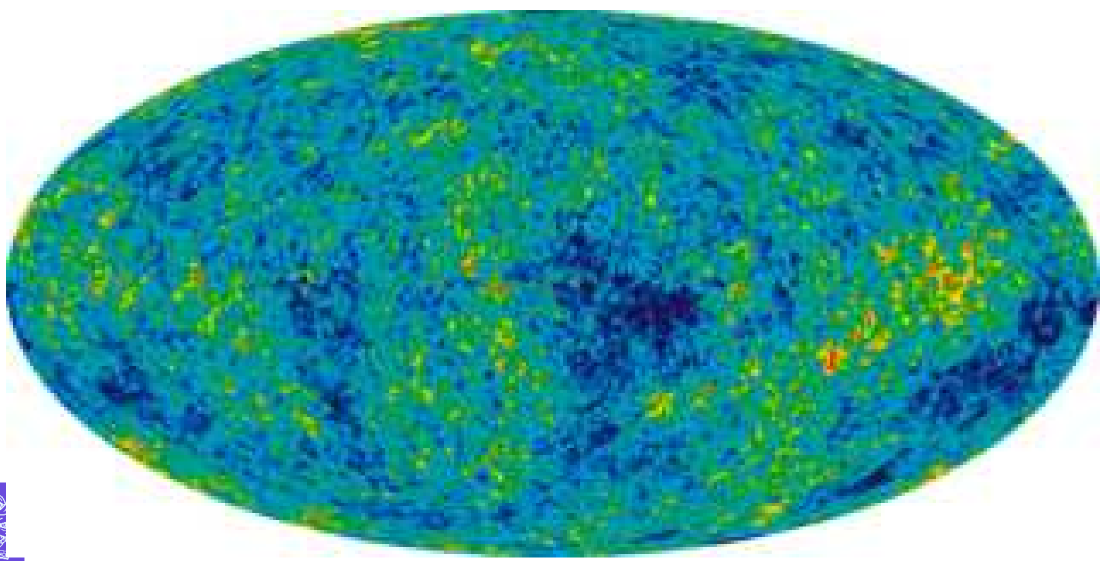

WMAP(2010) temperature anisotropy data $\Delta T \simeq 10^{-5} T$

CMBR Angular Correlations

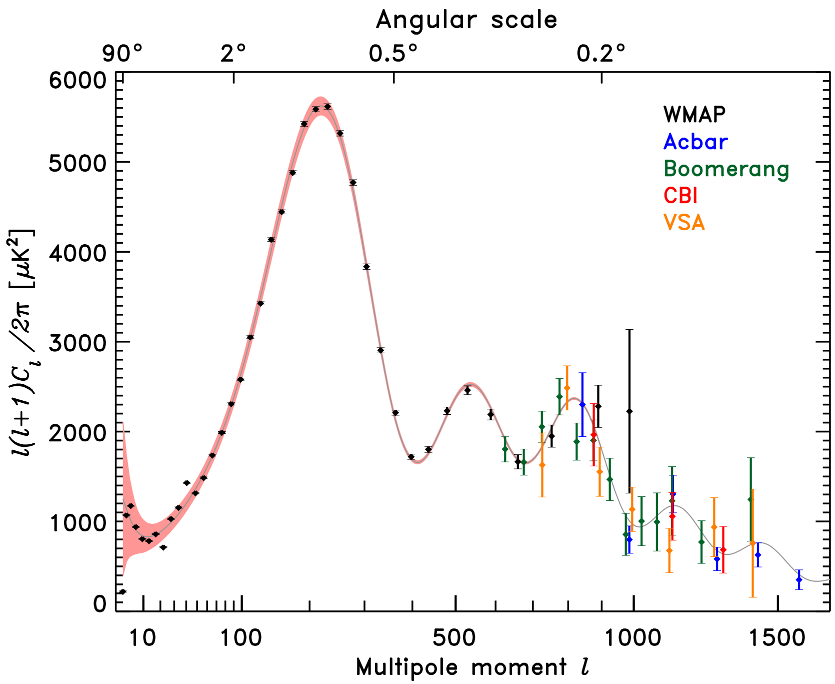

Temperature correlations (scalar) arise from the density fluctuations at the last scattering surface.

The data are accurate, and fit well to predictions of inflationary models.

CMBR Angular Correlations

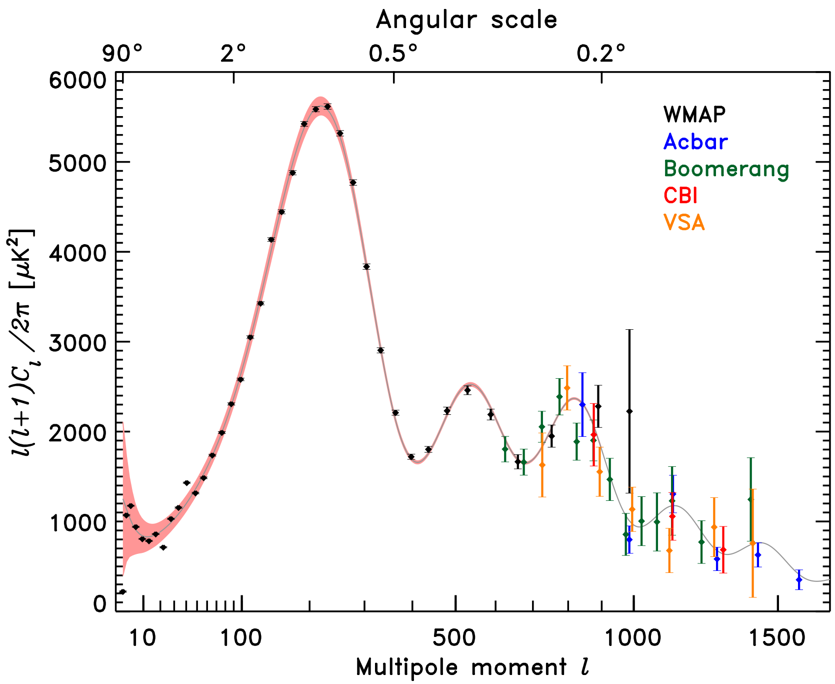

Temperature correlations (scalar) arise from the density fluctuations at the last scattering surface.

The data are accurate, and fit well to predictions of inflationary models.

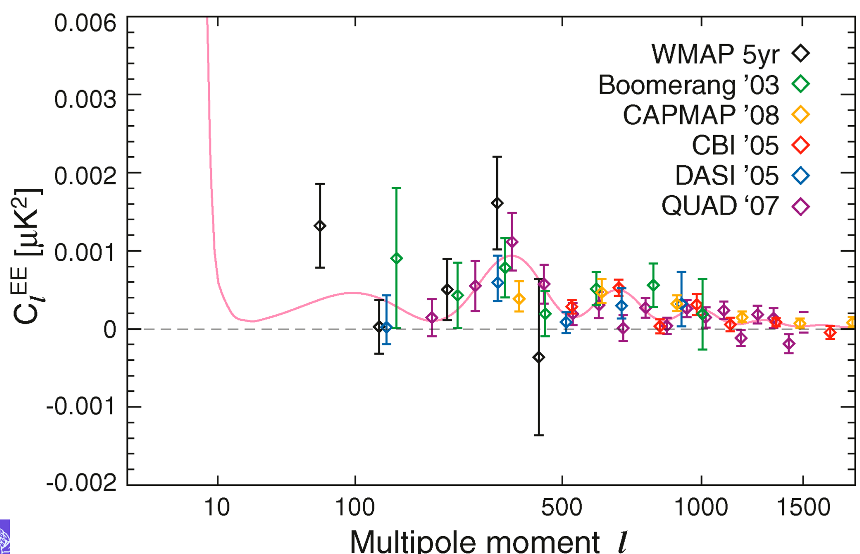

Polarisation correlations (tensor) arise from scattering in the plasma at the last scattering surface.

The data are poor.

Fireball Evolution Stages

(1) Collisions are dominated by low$-x$ high density gluons. Coherent saturated gluons form Colour Glass Condensate.

$\tau < 0.1$ fm/c

Fireball Evolution Stages

(1) Collisions are dominated by low$-x$ high density gluons. Coherent saturated gluons form Colour Glass Condensate.

$\tau < 0.1$ fm/c

(2) Strong longitudinal colour electric and colour magnetic fields relax. Non-zero impact parameter produces elliptic flow in the overlap region. Topological excitations and energy density fluctuations in the Glasma thermalise by hydrodynamic evolution.

$\tau = 0.1 - 1$ fm/c

Fireball Evolution Stages

(1) Collisions are dominated by low$-x$ high density gluons. Coherent saturated gluons form Colour Glass Condensate.

$\tau < 0.1$ fm/c

(2) Strong longitudinal colour electric and colour magnetic fields relax. Non-zero impact parameter produces elliptic flow in the overlap region. Topological excitations and energy density fluctuations in the Glasma thermalise by hydrodynamic evolution.

$\tau = 0.1 - 1$ fm/c

(3) Quasi-equilibrium quark-gluon plasma has energy density $\epsilon \simeq 1\mathrm{GeV}/\mathrm{fm}^3$ and $T_{\mathrm{cr}} \simeq 175\mathrm{MeV}$.

$\tau = 1 - 10$ fm/c

Fireball Evolution Stages

(1) Collisions are dominated by low$-x$ high density gluons. Coherent saturated gluons form Colour Glass Condensate.

$\tau < 0.1$ fm/c

(2) Strong longitudinal colour electric and colour magnetic fields relax. Non-zero impact parameter produces elliptic flow in the overlap region. Topological excitations and energy density fluctuations in the Glasma thermalise by hydrodynamic evolution.

$\tau = 0.1 - 1$ fm/c

(3) Quasi-equilibrium quark-gluon plasma has energy density $\epsilon \simeq 1\mathrm{GeV}/\mathrm{fm}^3$ and $T_{\mathrm{cr}} \simeq 175\mathrm{MeV}$.

$\tau = 1 - 10$ fm/c

(4) Hadronisation reduces entropy density and expands the fireball. Inelastic scattering stops, and species abundances get fixed, by chemical freeze-out at $T_{\mathrm{chem}} \simeq 170\mathrm{MeV}$.

$\tau > 10$ fm/c

Fireball Evolution Stages

(1) Collisions are dominated by low$-x$ high density gluons. Coherent saturated gluons form Colour Glass Condensate.

$\tau < 0.1$ fm/c

(2) Strong longitudinal colour electric and colour magnetic fields relax. Non-zero impact parameter produces elliptic flow in the overlap region. Topological excitations and energy density fluctuations in the Glasma thermalise by hydrodynamic evolution.

$\tau = 0.1 - 1$ fm/c

(3) Quasi-equilibrium quark-gluon plasma has energy density $\epsilon \simeq 1\mathrm{GeV}/\mathrm{fm}^3$ and $T_{\mathrm{cr}} \simeq 175\mathrm{MeV}$.

$\tau = 1 - 10$ fm/c

(4) Hadronisation reduces entropy density and expands the fireball. Inelastic scattering stops, and species abundances get fixed, by chemical freeze-out at $T_{\mathrm{chem}} \simeq 170\mathrm{MeV}$.

$\tau > 10$ fm/c

(5) Elastic and resonant scattering (mediated largely by pions) ceases, with kinetic freeze-out at $T_{\mathrm{kin}} \simeq 120\mathrm{MeV}$.

Experimental Signals

Multiplicities and distributions of various particles are detected. Only charged hadrons observed in sufficiently transverse directions (to avoid the unscattered beams).

Photons and leptons are also observed through their electromagnetic interactions.

Glauber model used to infer the centrality of the collisions (no. of participants) from the charged particle multiplicities.

Experimental Signals

Multiplicities and distributions of various particles are detected. Only charged hadrons observed in sufficiently transverse directions (to avoid the unscattered beams).

Photons and leptons are also observed through their electromagnetic interactions.

Glauber model used to infer the centrality of the collisions (no. of participants) from the charged particle multiplicities.

(a) Initial approach to equilibrium signals: Direct photons and leptons, heavy quark jets, high p_T jets, the elliptic flow.
(b) Quasi-equilibrated QGP signals: Moderate p_T hadrons produced close to the fireball surface.

Experimental Signals

Multiplicities and distributions of various particles are detected. Only charged hadrons observed in sufficiently transverse directions (to avoid the unscattered beams).

Photons and leptons are also observed through their electromagnetic interactions.

Glauber model used to infer the centrality of the collisions (no. of participants) from the charged particle multiplicities.

(a) Initial approach to equilibrium signals: Direct photons and leptons, heavy quark jets, high p_T jets, the elliptic flow.
(b) Quasi-equilibrated QGP signals: Moderate p_T hadrons produced close to the fireball surface.

Temperature information is extracted from particle abundances ($T_{\rm chem}$) and energy-momentum distributions ($T_{\rm kin}$), using thermalised hadron resonance gas models.

Angular distributions can see through the scatterings to the correlation patterns in the QGP (assuming low diffusion).

Types of observables

Specific patterns in the distribution of hadrons can be searched for, using techniques similar to those used to analyse the temperature fluctuations in the CMBR.

Types of observables

Specific patterns in the distribution of hadrons can be searched for, using techniques similar to those used to analyse the temperature fluctuations in the CMBR.

One-point observables:

Particle multiplicities (enhancements, suppressions)
Particle number fluctuations (susceptibilities)
Distributions of conserved charges ($n_u, n_d, n_s \leftrightarrow Q, B, S$)
Energy-momentum distributions and jets
Angular distributions (elliptic flow and harmonics)

Types of observables

Specific patterns in the distribution of hadrons can be searched for, using techniques similar to those used to analyse the temperature fluctuations in the CMBR.

One-point observables:

Particle multiplicities (enhancements, suppressions)
Particle number fluctuations (susceptibilities)
Distributions of conserved charges ($n_u, n_d, n_s \leftrightarrow Q, B, S$)
Energy-momentum distributions and jets
Angular distributions (elliptic flow and harmonics)

Two-point observables:

Angular correlations for particles and charges
(e.g. ridge, jet quenching, Hanbury-Brown–Twiss effect)

Sum rules relate two-point observables to one-point ones (e.g. correlations to susceptibilities).

QCD Phase Structure

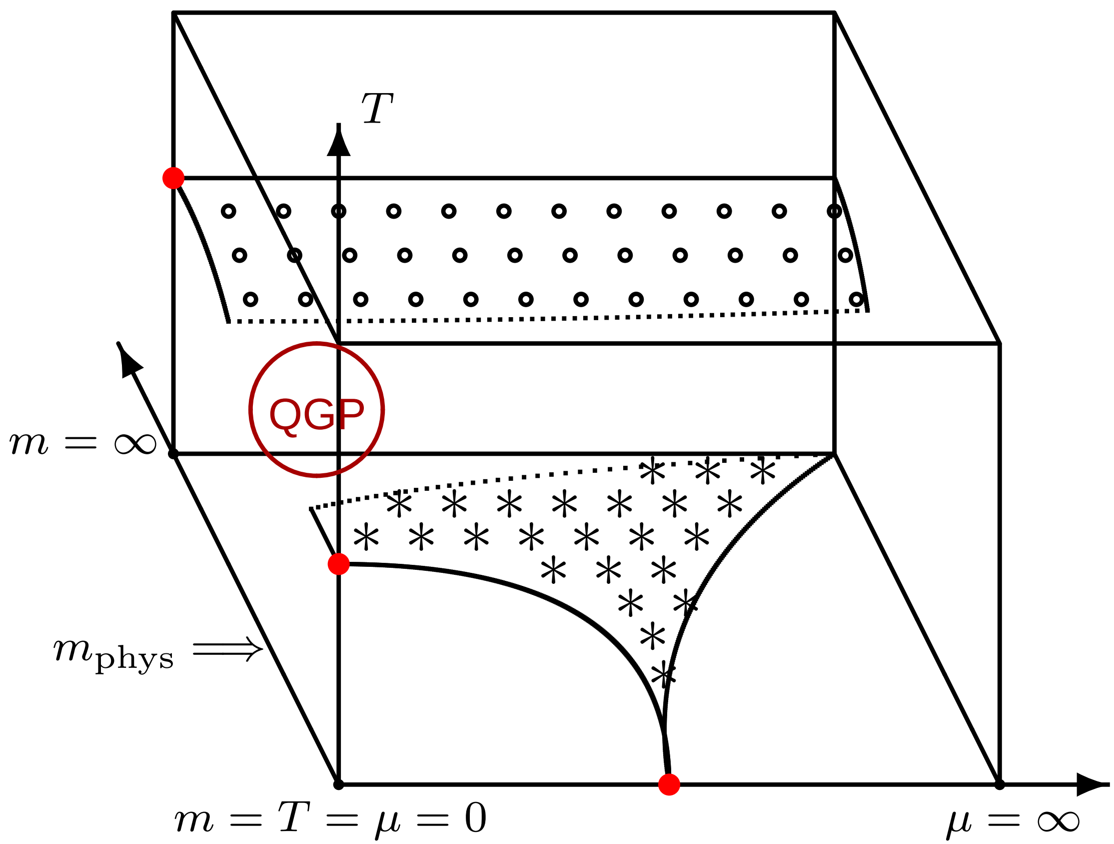

Schematic description of the phase structure of QCD in the $m - T - \mu$ space.

First order transition surfaces are shown shaded, and critical lines are shown dotted.

Colour superconductor phases occurring at large chemical potential are omitted.

RHIC and LHC experiments belong to the cross-over region.

QCD Phase Transitions

(1) $m = \infty$, $N \geq 3$: First order finite temperature deconfinement transition, governed by the breaking of the global Z_N centre symmetry of the Polyakov loop.

(2) $m = 0 = \mu$, $N_f \geq 3$: First order finite temperature chiral transition, governed by the restoration of the flavour $SU(N_f)_V$ symmetry to $SU(N_f)_L \otimes SU(N_f)_R$.

(3) $m = 0 = T$, $\mu \simeq$ constituent quark mass: First order baryon condensation phase transition, where the vacuum structure changes from $\langle\bar{\psi}\psi\rangle \neq 0$ to $\langle\psi^\dagger\psi\rangle \neq 0$.

First order phase transitions are stable against small changes of symmetry breaking perturbations. The above three transitions extend inward, to varying extent, from the boundaries of the phase structure.

No phase transition for the physical values of the quark masses (unless μ is sufficiently large). But the three nearby transitions produce their imprints in the cross-over region.

Flux Tubes in QCD

QCD exhibits dual superconductivity with linearly confined colour-electric flux. (Nambu, ’t Hooft, Mandelstam)

Lattice QCD calculations show area law for Wilson loops, analytically at strong coupling and numerically at weak coupling. The characteristic scale is $r \geq 0.5$ fm.

Flux Tubes in QCD

QCD exhibits dual superconductivity with linearly confined colour-electric flux. (Nambu, 't Hooft, Mandelstam)

Lattice QCD calculations show area law for Wilson loops, analytically at strong coupling and numerically at weak coupling. The characteristic scale is $r \geq 0.5$ fm.

Meson and baryon wavefunctions are represented by the invariant tensors δ_{ab} and ϵ_{abc}. Other multi-quark hadrons (except for nuclei) are phenomenologically not prominent.

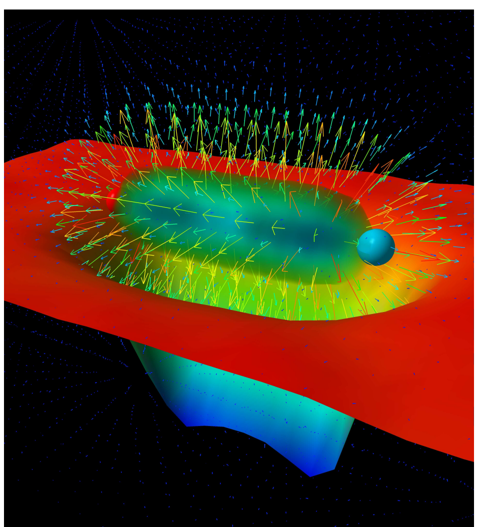

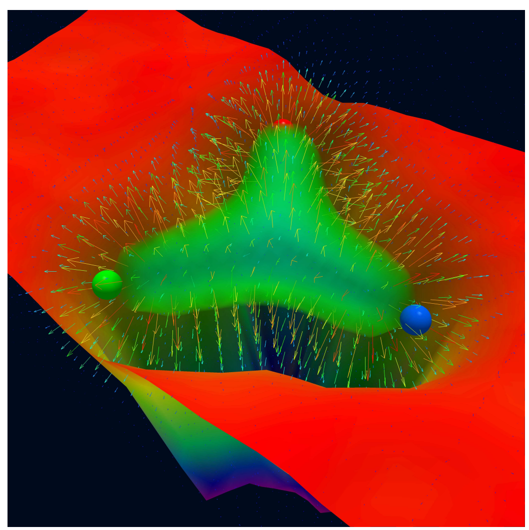

F. Bissey, F.G. Cao, A.R. Kitson, A.I Signal, D.B. Leinweber, B.G. Lassock and A.G. Williams, Phys. Rev. D 76 (2007) 114512.

Flux Tube Configurations

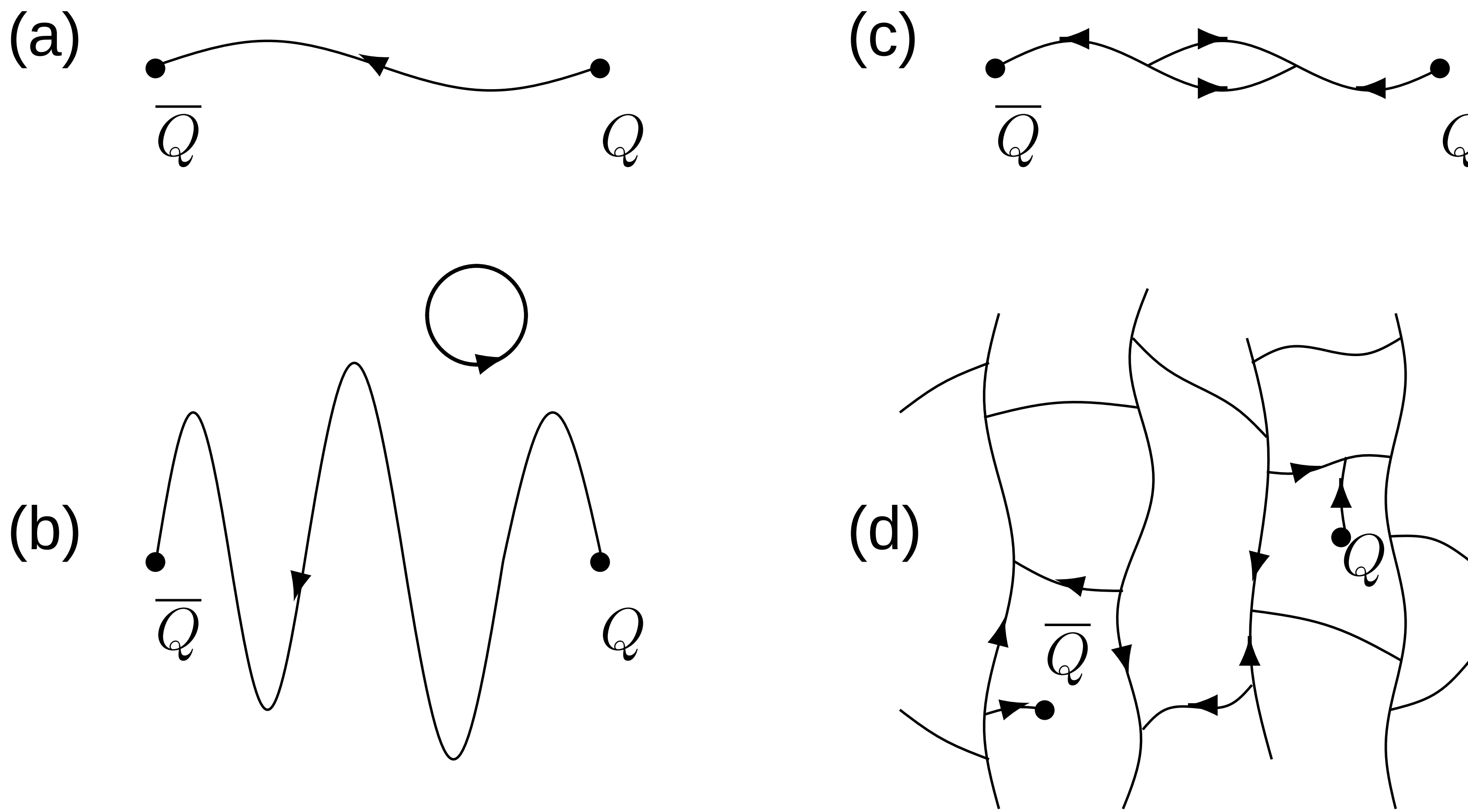

Possible flux tube configurations connecting a static quark-antiquark pair, as the temperature is increased (from top to bottom), and when baryonic vertices are included (from left to right).

Flux Tube Breaking

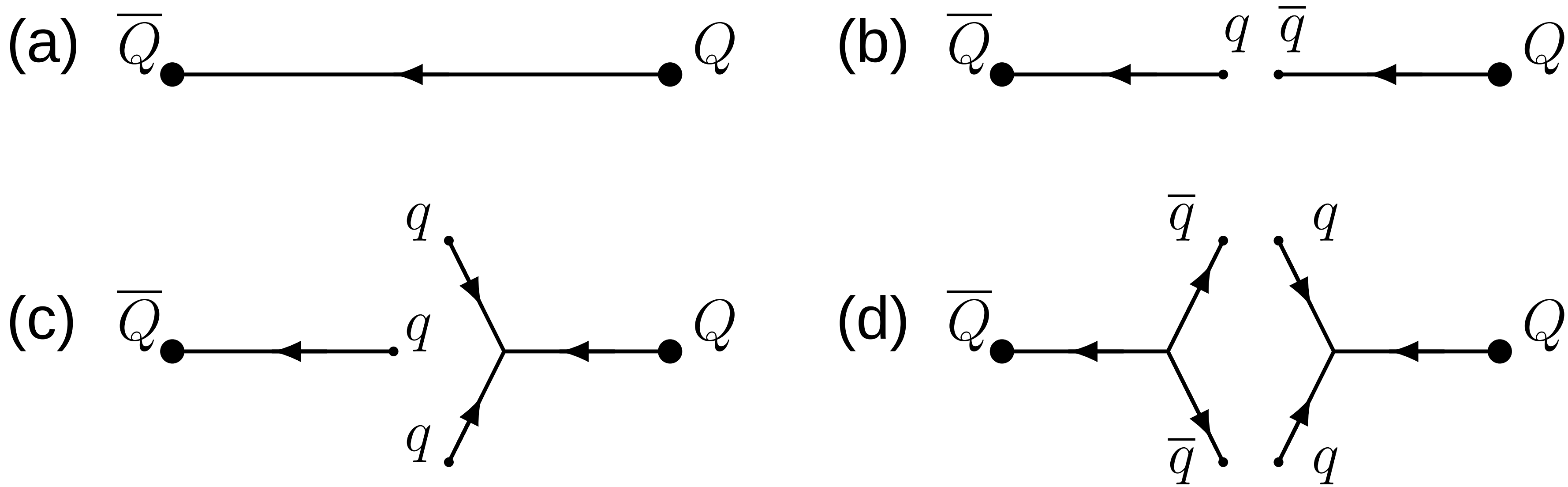

A colour-electric flux tube can break when dynamical quarks are included in QCD.

(a) A flux tube produced by static colour sources.

(b) Its breaking by a quark-antiquark pair appearing from the vacuum.

(c) Its breaking by a baryon appearing from the vacuum at finite chemical potential.

(d) Breaking of a vertex-antivertex flux tube bubble by two quark-antiquark pairs.

[In reality, baryon number is conserved, and baryon-antibaryon pairs are produced. Hadronization models incorporate that using effective diquark degrees of freedom.]

Deconfinement Phase Transition

Finite temperature behaviour of QCD is governed by the competition between energy and entropy of the flux tube configurations.

With increasing temperature, the flux tubes oscillate more in space, and also produce more vertices.

Deconfinement means a quark-antiquark pair loses information about each-other's position.

Deconfinement Phase Transition

Finite temperature behaviour of QCD is governed by the competition between energy and entropy of the flux tube configurations.

With increasing temperature, the flux tubes oscillate more in space, and also produce more vertices.

Deconfinement means a quark-antiquark pair loses information about each-other's position.

Second order phase transition corresponds to flux tubes of diverging length. First order phase transition corresponds to a percolating flux tube network.

Deconfinement Phase Transition

Finite temperature behaviour of QCD is governed by the competition between energy and entropy of the flux tube configurations.
With increasing temperature, the flux tubes oscillate more in space, and also produce more vertices.
Deconfinement means a quark-antiquark pair loses information about each-other's position.

Second order phase transition corresponds to flux tubes of diverging length. First order phase transition corresponds to a percolating flux tube network.

Light dynamical quarks break up long flux tubes, changing the deconfinement phase transition into a cross-over.
Still large enough clusters of flux tubes may arise at m_{phys}, as a consequence of the nearby phase transition.

Flux Tube Model Variables

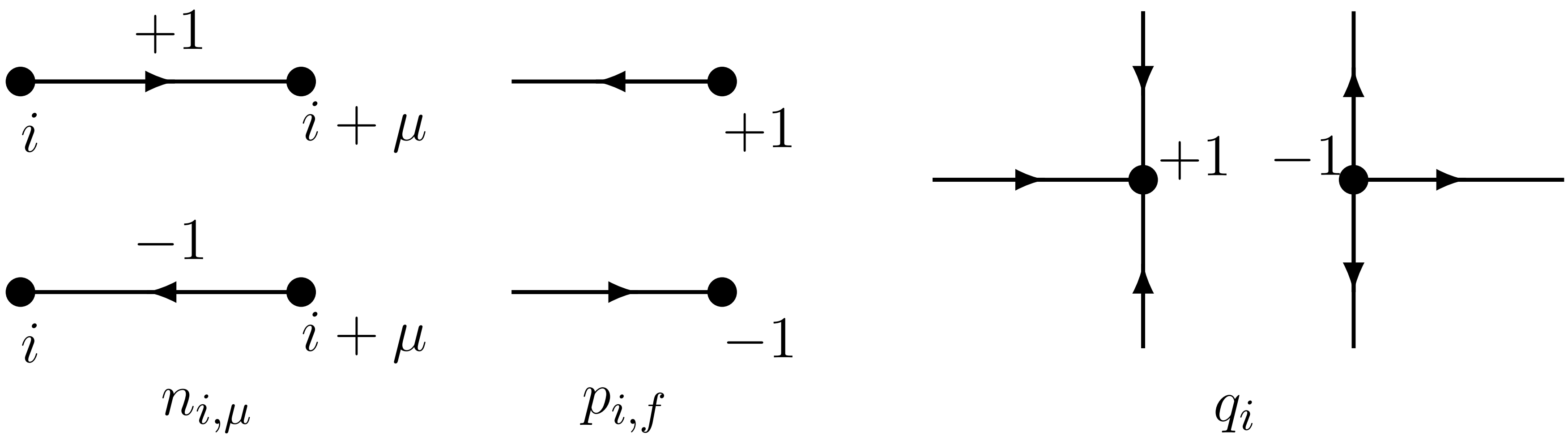

The link and site variables for the flux tube model.

Energy: $E = \sigma a \sum_{i,\mu} |n_{i,\mu}| + m \sum_{i,f} |p_{i,f}| + v \sum_i |q_i|$

Gauss's Law: $\sum_\mu (n_{i,\mu} - n_{i-\mu,\mu}) - \sum_f p_{i,f} + N q_i \equiv \alpha_i = 0$

Baryon Number: $B = \frac{1}{N} \sum_{i,f} p_{i,f} = \sum_i q_i$

Grand Canonical Partition Function

$$Z[T,\mu] = \sum_{n_{i,\mu},\ p_{i,f},\ q_i} \exp\left[-\frac{1}{T}(E - \mu NB)\right] \prod_i \delta_{\alpha_i,0}$$

The constraint can be solved by changing to dual variables:

$$\delta_{\alpha_i,0} = \int_{-\pi}^{\pi} \frac{d\theta_i}{2\pi}\ e^{i\alpha_i\theta_i}$$

Sum over $n_{i,\mu},\ p_{i,f},\ q_i$ can then be explicitly carried out:

$$Z[T,\mu] = \int_{-\pi}^{\pi} \prod_i \frac{d\theta_i}{2\pi}\ \prod_{i,\mu} (1 + 2e^{-\sigma a/T}\cos(\theta_{i+\mu} - \theta_i)) \times$$

$$\times \prod_i \left(1 + 2e^{-m/T}\cos\left(\theta_i + i\frac{\mu}{T}\right)\right)^{2N_f} \prod_i (1 + 2e^{-v/T}\cos(N\theta_i))$$

Phenomenological Features

The model is in the universality class of the XY spin model, with an ordinary and a $Z(N)$ symmetric magnetic field.

$$Z[T,\mu] = \int_{-\pi}^{\pi} \prod_i \frac{d\theta_i}{2\pi} \; \exp\Big[J \sum_{i,\mu} \cos(\theta_{i+\mu} - \theta_i) +$$

$$+ h \sum_i \cos\left(\theta_i + i\frac{\mu}{T}\right) + p \sum_i \cos(N\theta_i) \Big]$$

$$J \simeq 2e^{-\sigma a/T} \;, \quad h \simeq 4N_f \; e^{-m/T} \;, \quad p \simeq 2e^{-v/T}$$

Phenomenological Features

The model is in the universality class of the XY spin model, with an ordinary and a $Z(N)$ symmetric magnetic field.

$$Z[T,\mu] = \int_{-\pi}^{\pi} \prod_i \frac{d\theta_i}{2\pi} \, \exp\Big[J \sum_{i,\mu} \cos(\theta_{i+\mu} - \theta_i) + \\ + h \sum_i \cos\left(\theta_i + i\frac{\mu}{T}\right) + p \sum_i \cos(N\theta_i) \Big]$$

$$J \simeq 2e^{-\sigma a/T} \, , \quad h \simeq 4N_f \, e^{-m/T} \, , \quad p \simeq 2e^{-v/T}$$

Introduction of a static quark source at site j modifies the Gauss's law constraint there as $\delta_{\alpha_j,0} \to \delta_{\alpha_j,-1}$.

Its free energy is given by $\exp(-F_q/T) = \langle \exp(-i\theta_j) \rangle$.

So θ_i corresponds to the phase of the Polyakov loop.

Flux tube and Polyakov loop descriptions of deconfinement in finite temperature gauge theory are dual to each other.

Correlations of vertices can be related to correlations of P^3.

Baryon Number Correlations

Focus on the position space picture of the flux tube network.

In every flux tube cluster, any neighbour of a vertex is an anti-vertex and vice versa. Production and annihilation of vertices stops at fragmentation stage. Thereafter, every vertex yields a baryon and every anti-vertex an antibaryon.

Baryon Number Correlations

Focus on the position space picture of the flux tube network.

In every flux tube cluster, any neighbour of a vertex is an anti-vertex and vice versa. Production and annihilation of vertices stops at fragmentation stage. Thereafter, every vertex yields a baryon and every anti-vertex an antibaryon.

In absence of large scale diffusion, radial propagation of (anti)baryons preserves the geometric pattern of (anti)vertices present at the chemical freeze-out stage.

Angular positions of (anti)baryons seen in the detector can be backtracked to the angular positions of (anti)vertices that emerge from the QGP fireball.

Baryon Number Correlations

Focus on the position space picture of the flux tube network.

In every flux tube cluster, any neighbour of a vertex is an anti-vertex and vice versa. Production and annihilation of vertices stops at fragmentation stage. Thereafter, every vertex yields a baryon and every anti-vertex an antibaryon.

In absence of large scale diffusion, radial propagation of (anti)baryons preserves the geometric pattern of (anti)vertices present at the chemical freeze-out stage.

Angular positions of (anti)baryons seen in the detector can be backtracked to the angular positions of (anti)vertices that emerge from the QGP fireball.

Bipartite graph:

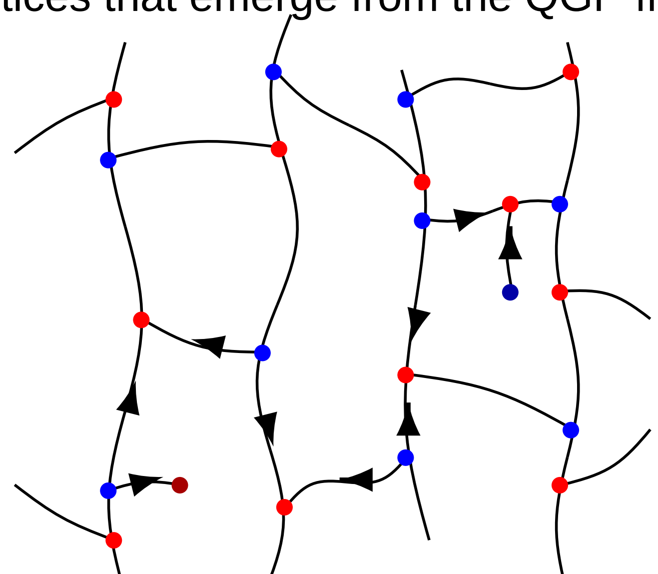

Observable Pattern

Arrangement of vertices and anti-vertices as alternating neighbours can yield an oscillatory signal in baryon number correlations, provided: (in a mimicry of the Sakharov conditions)

(1) A mechanism for local baryon-antibaryon pair production exists. This is inherent in QCD dynamics.

Observable Pattern

Arrangement of vertices and anti-vertices as alternating neighbours can yield an oscillatory signal in baryon number correlations, provided: (in a mimicry of the Sakharov conditions)

(1) A mechanism for local baryon-antibaryon pair production exists. This is inherent in QCD dynamics.

(2) The system has a non-zero chemical potential (i.e. a Fermi surface). This avoids spectral positivity constraints, and is true in experiments.

Observable Pattern

Arrangement of vertices and anti-vertices as alternating neighbours can yield an oscillatory signal in baryon number correlations, provided: (in a mimicry of the Sakharov conditions)

(1) A mechanism for local baryon-antibaryon pair production exists. This is inherent in QCD dynamics.

(2) The system has a non-zero chemical potential (i.e. a Fermi surface). This avoids spectral positivity constraints, and is true in experiments.

(3) The dynamical evolution is not in equilibrium. This favours fragmentation of flux tube clusters, while suppressing vertex-antivertex annihiliation. Production of a sizeable number of antibaryons in experiments, from an initial state that has none, confirms it.

Pair Distribution Function

Density: $\rho(\vec{r}) = \left\langle \sum_\alpha \delta(\vec{r} - \vec{r}_i) \right\rangle$

Correlation: $\rho(\vec{r})\ g(\vec{r}, \vec{r}')\ \rho(\vec{r}') = \left\langle \sum_{i \neq j} \delta(\vec{r} - \vec{r}_i)\ \delta(\vec{r}' - \vec{r}_j) \right\rangle$

In homogeneous and isotropic fluids, ρ is independent of $\vec{r}$ and g depends only on $|\vec{r} - \vec{r}'|$, resulting in

$$\rho\ g(r) = \left\langle \sum_{i \neq 0} \delta(\vec{r} - \vec{r}_i) \right\rangle$$

Pair Distribution Function

Density: $\rho(\vec{r}) = \left\langle \sum_\alpha \delta(\vec{r} - \vec{r}_i) \right\rangle$

Correlation: $\rho(\vec{r})\; g(\vec{r}, \vec{r}')\; \rho(\vec{r}') = \left\langle \sum_{i \neq j} \delta(\vec{r} - \vec{r}_i)\; \delta(\vec{r}' - \vec{r}_j) \right\rangle$

In homogeneous and isotropic fluids, ρ is independent of $\vec{r}$ and g depends only on $|\vec{r} - \vec{r}'|$, resulting in

$$\rho\; g(r) = \left\langle \sum_{i \neq 0} \delta(\vec{r} - \vec{r}_i) \right\rangle$$

Asymptotically, $g(r \to \infty) = 1$ (interactions fade away).

For an ideal gas with no correlations, $g(r) = 1$.

For objects with hard-core repulsion, $g(0) = 0$, and beyond the hard core $g(r)$ tends to its asymptotic value 1, exhibiting damped oscillations.

Pair Distribution Function

Density: $\rho(\vec{r}) = \left\langle \sum_\alpha \delta(\vec{r} - \vec{r}_i) \right\rangle$

Correlation: $\rho(\vec{r})\ g(\vec{r}, \vec{r}')\ \rho(\vec{r}') = \left\langle \sum_{i \neq j} \delta(\vec{r} - \vec{r}_i)\ \delta(\vec{r}' - \vec{r}_j) \right\rangle$

In homogeneous and isotropic fluids, ρ is independent of $\vec{r}$ and g depends only on $|\vec{r} - \vec{r}'|$, resulting in

$$\rho\ g(r) = \left\langle \sum_{i \neq 0} \delta(\vec{r} - \vec{r}_i) \right\rangle$$

Asymptotically, $g(r \to \infty) = 1$ (interactions fade away).
For an ideal gas with no correlations, $g(r) = 1$.
For objects with hard-core repulsion, $g(0) = 0$, and beyond the hard core $g(r)$ tends to its asymptotic value 1, exhibiting damped oscillations.

For baryon number distributions, $g_{|v|}$ is a correlation insensitive reference function, while g_v (vertex signs $q_i q_j$ included) is sensitive to vertex-antivertex correlations.
The contrast between the two measures the correlations.

Theoretical Expectations

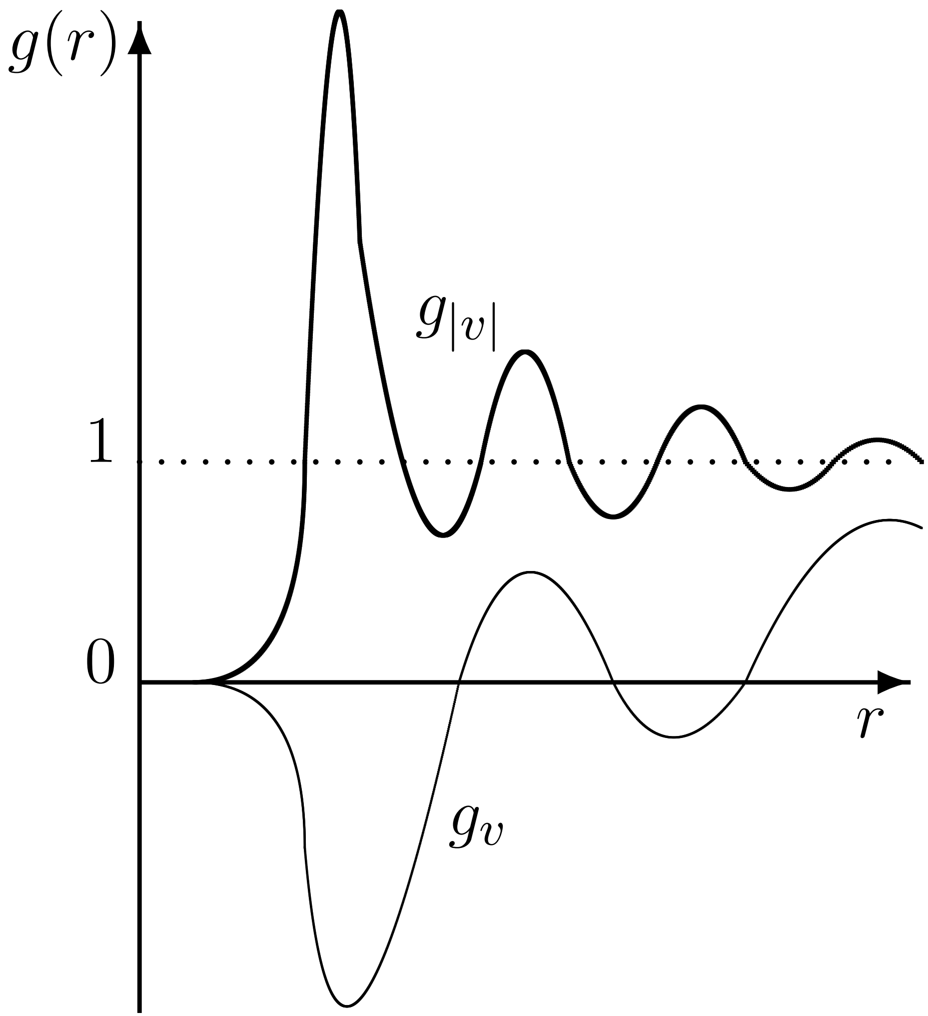

Positions of peaks quantify separations of neighbours.

Widths of peaks measure hard/soft nature of objects.

The first peak is the most informative.

Liquids have longer range correlations than gases.

Schematic representation of the pair distribution functions $g_{|v|}(r)$ and $g_v(r)$. The former is similar to that for objects with hard-core repulsion. The latter is for a percolating flux tube network where vertices and anti-vertices alternate (similar to $\pm$ charges in ionic liquids).

Gaps Between Theory and Experiment

Major hurdle:

Detectors observe protons and anti-protons, but not neutrons and anti-neutrons. Baryon number correlations can be extracted only if the observed subset is a faithful representation (ideally proportional) of the total distribution.

Gaps Between Theory and Experiment

Major hurdle:
Detectors observe protons and anti-protons, but not neutrons and anti-neutrons. Baryon number correlations can be extracted only if the observed subset is a faithful representation (ideally proportional) of the total distribution.

There are other practical corrections.
Correlations are weakened by:
(1) Only approximate equilibration of the fireball,
(2) Non-uniformity of the QGP due to the elliptic flow,
(3) Baryon number diffusion after hadronisation,
and strengthened by:
(4) Development of hard baryon core during hadronisation.

Gaps Between Theory and Experiment

Major hurdle:
Detectors observe protons and anti-protons, but not neutrons and anti-neutrons. Baryon number correlations can be extracted only if the observed subset is a faithful representation (ideally proportional) of the total distribution.

There are other practical corrections.
Correlations are weakened by:
(1) Only approximate equilibration of the fireball,
(2) Non-uniformity of the QGP due to the elliptic flow,
(3) Baryon number diffusion after hadronisation,
and strengthened by:
(4) Development of hard baryon core during hadronisation.

Low diffusion and low viscosity are compatible because of high entropy of hadronic medium.
Einstein-Stokes relation: $D = kT/(6\pi\eta r)$. For the RHIC and LHC data:

$\eta/s \lesssim 0.4\hbar/k$, $\eta = 5 \times 10^{11}$Pa.s, $r = 1$fm, $T = 170$MeV $\Rightarrow D = 10^{-2}$c.fm

Despite these gaps . . .

(a) There is no fundamental interaction associated with the baryon number. So the correlations have to arise from the preceding dynamics of QCD in the QGP phase.
(b) The vertex-antivertex correlation is a topological feature, robust against many details of the dynamics.

Despite these gaps . . .

(a) There is no fundamental interaction associated with the baryon number. So the correlations have to arise from the preceding dynamics of QCD in the QGP phase.
(b) The vertex-antivertex correlation is a topological feature, robust against many details of the dynamics.

Correlation signal parameters:
(1) Peak position (interbaryon separation): $\simeq 2$fm.

Fireball radius in central heavy ion collisions is ~ 6fm.

(2) Peak height (tightness of packing): Estimate needed.
(3) Axial symmetry (improving the signal): Decomposition into orthogonal azimuthal and parity components can help.

Despite these gaps . . .

(a) There is no fundamental interaction associated with the baryon number. So the correlations have to arise from the preceding dynamics of QCD in the QGP phase.
(b) The vertex-antivertex correlation is a topological feature, robust against many details of the dynamics.

Correlation signal parameters:
(1) Peak position (interbaryon separation): $\simeq 2$fm.

Fireball radius in central heavy ion collisions is ~ 6fm.

(2) Peak height (tightness of packing): Estimate needed.
(3) Axial symmetry (improving the signal): Decomposition into orthogonal azimuthal and parity components can help.

It is worthwhile to look for the two-point baryon number correlations in the experimental data, as a characteristic signature of the deconfinement phase transition, without worrying about accurate prediction of its magnitude.

Hadronisation

Now consider the non-equilibrium QCD evolution as the quark-gluon plasma cools from above T_{cr} to $T = 0$.

The initial fireball state is dominated by gluons.
Gluons also equilibriate faster than quarks due to their larger colour charge (adjoint vs. fundamental).

So we assume that a flux tube network would be a reasonable description of the fireball above T_{cr}.

Hadronisation

Now consider the non-equilibrium QCD evolution as the quark-gluon plasma cools from above $T_{\rm cr}$ to $T=0$.

The initial fireball state is dominated by gluons. Gluons also equilibriate faster than quarks due to their larger colour charge (adjoint vs. fundamental).

So we assume that a flux tube network would be a reasonable description of the fireball above $T_{\rm cr}$.

Expanding fireball and decreasing temperature break up the flux tube segments by quark-antiquark pair creation. The fragments end up as mesons and baryons.

This fragmentation is governed by the constituent quark (not hadron) dynamics, and fixes the chemical equilibrium.

Spin configurations settle down later by elastic scattering, fixing hyperfine interactions and hadron identities.

Hadron Multiplicities

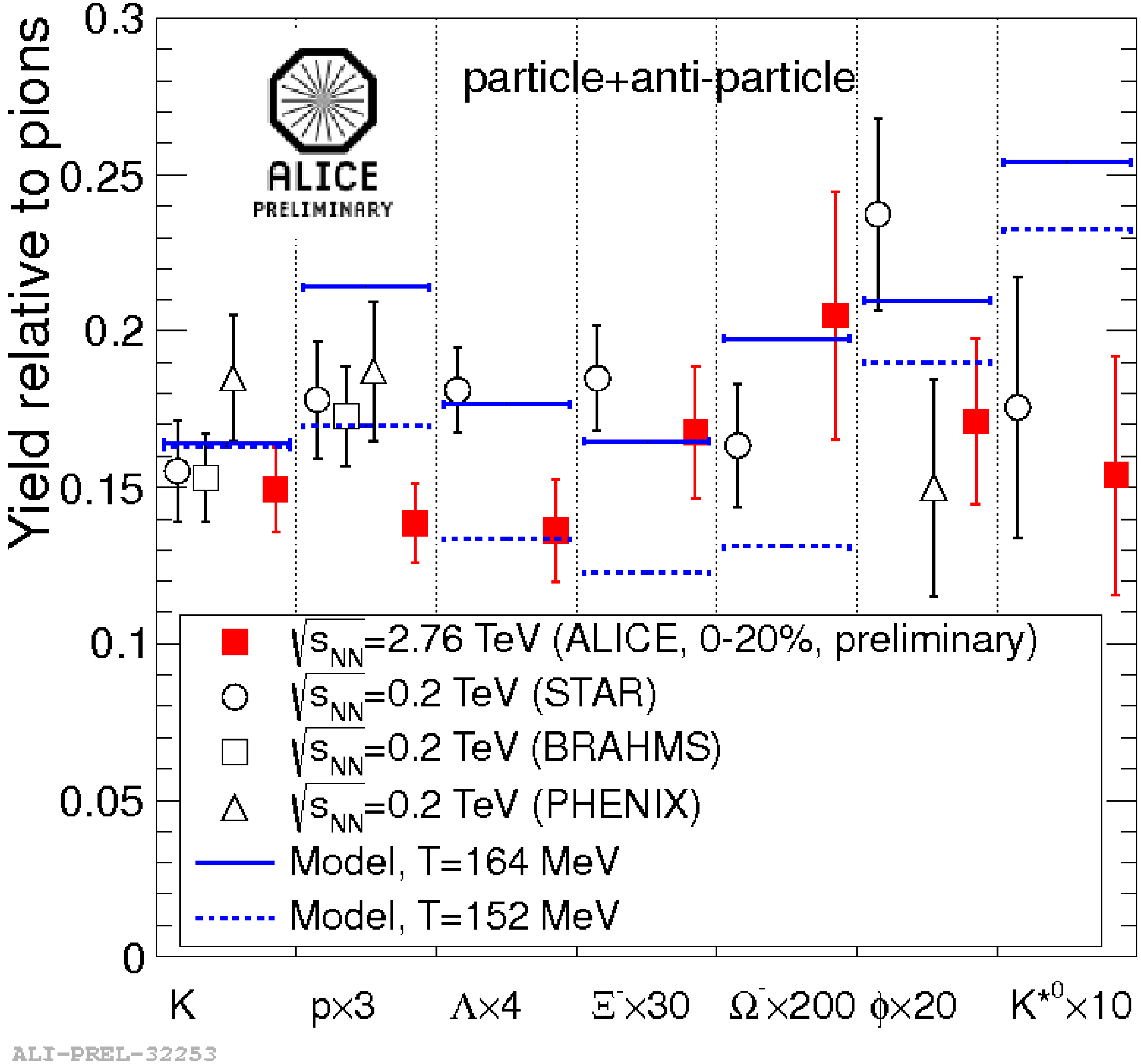

There is a systematic mismatch between observed and predicted baryon multiplicities, i.e. enhanced strangeness production, when thermal models with experimental hadron masses are used.

L. Milano (ALICE Collaboration), Nucl. Phys. A 904-905 (2013) 531c.

Model for Hadron Multiplicities

Experimentally identified hadrons emerging from the fireball are $\pi^{\pm}$, $K^{\pm}$, $p(\overline{p})$, $\Lambda(\overline{\Lambda})$, $\Xi^{-}(\overline{\Xi}^{+})$, $\Omega^{-}(\overline{\Omega}^{+})$ and ϕ.

Other hadrons either decay too fast or escape the detectors.

Relative abundances of hadrons with different flavour structure are fixed at the chemical equilibrium stage.

Subsequent quark-antiquark annihiliation is negligible.

Model for Hadron Multiplicities

Experimentally identified hadrons emerging from the fireball are $\pi^\pm$, $K^\pm$, $p(\overline{p})$, $\Lambda(\overline{\Lambda})$, $\Xi^-(\overline{\Xi}^+)$, $\Omega^-(\overline{\Omega}^+)$ and ϕ.

Other hadrons either decay too fast or escape the detectors.

Relative abundances of hadrons with different flavour structure are fixed at the chemical equilibrium stage.

Subsequent quark-antiquark annihiliation is negligible.

Quark-antiquark pair production probabilities are governed by the flavour dependent weights:

$$f_i = [1 + e^{(E-\mu_i)/T}]^{-1}, \quad E^2 = p^2 + m_i^2, \quad \mu_i \ll T \ ,$$

integrated over the phase space.

Model for Hadron Multiplicities

Experimentally identified hadrons emerging from the fireball are $\pi^{\pm}$, $K^{\pm}$, $p(\overline{p})$, $\Lambda(\overline{\Lambda})$, $\Xi^{-}(\overline{\Xi}^{+})$, $\Omega^{-}(\overline{\Omega}^{+})$ and ϕ.

Other hadrons either decay too fast or escape the detectors.

Relative abundances of hadrons with different flavour structure are fixed at the chemical equilibrium stage.

Subsequent quark-antiquark annihiliation is negligible.

Quark-antiquark pair production probabilities are governed by the flavour dependent weights:

$$f_i = [1 + e^{(E-\mu_i)/T}]^{-1}, \quad E^2 = p^2 + m_i^2, \quad \mu_i \ll T \ ,$$

integrated over the phase space.

The number of times a flux tube segment between vertices breaks determines the proportion of mesons to baryons.

The model parameters are string tension (σ), quark masses (m_i) and vertex energy (v).

Constituent Quark Mass Fit

ALICE: The experimentally observed hadron ratios are

$\pi^{\pm}$	$K^{\pm}$	p	Λ	Ξ^{-}	Ω^{-}	ϕ
1.0	0.15(1)	0.046(4)	0.034(4)	0.0056(7)	0.00102(20)	0.0086(13)

Constituent quark masses that fit the hadron spectrum with hyperfine splittings are: $m_l \approx 340$ MeV, $m_s \approx 510$ MeV.

Constituent Quark Mass Fit

ALICE: The experimentally observed hadron ratios are

$\pi^\pm$	$K^\pm$	p	Λ	Ξ^-	Ω^-	ϕ
1.0	0.15(1)	0.046(4)	0.034(4)	0.0056(7)	0.00102(20)	0.0086(13)

Constituent quark masses that fit the hadron spectrum with hyperfine splittings are: $m_l \approx 340$ MeV, $m_s \approx 510$ MeV.

Baryons: Flavour counting for $(10+8)$-plets, with decays according to the PDG data and isospin factors, predicts

$$p : n : \Lambda : \Xi^- : \Omega^- = 3.56 : 4.68 : 6.76y : 2y^2 : y^3,$$

where y is the suppression factor for strange quark production relative to that for light quarks.

Constituent Quark Mass Fit

ALICE: The experimentally observed hadron ratios are

$\pi^\pm$	$K^\pm$	p	Λ	Ξ^-	Ω^-	ϕ
1.0	0.15(1)	0.046(4)	0.034(4)	0.0056(7)	0.00102(20)	0.0086(13)

Constituent quark masses that fit the hadron spectrum with hyperfine splittings are: $m_l \approx 340$ MeV, $m_s \approx 510$ MeV.

Baryons: Flavour counting for $(10+8)$-plets, with decays according to the PDG data and isospin factors, predicts

$$p : n : \Lambda : \Xi^- : \Omega^- = 3.56 : 4.68 : 6.76y : 2y^2 : y^3,$$

where y is the suppression factor for strange quark production relative to that for light quarks.

Fit: $y = 0.43$, with proton to pion ratio of 0.046, gives

$$p : \Lambda : \Xi^- : \Omega^- = 0.046 : 0.038 : 0.0048 : 0.00103.$$

Note that $e^{-(m_s - m_l)/T_{\rm cr}} \sim 0.35$. $\langle f_s/f_l \rangle$ is somewhat larger.

Alternative explanations have been proposed.
They all treat light and strange quarks differently.

1. Final state interactions with $p\bar{p}$ annihiliations.
2. Unequal freeze-out temperatures for u, d and s quarks.
3. Unequal excluded volumes for light and strange hadrons.

Alternative explanations have been proposed.
They all treat light and strange quarks differently.

1. Final state interactions with $p\overline{p}$ annihiliations.
2. Unequal freeze-out temperatures for u, d and s quarks.
3. Unequal excluded volumes for light and strange hadrons.

Other Applications

Flux tube vertices provide an intuitive way to incorporate baryons in QCD fragmentation/hadronisation models (in contrast to ad hoc degrees of freedom such as diquarks).

Existing models have trouble fitting baryonic observables.

Going beyond one-dimensional string picture may improve predictive power of PYTHIA (Lund string model), HIJING, HERWIG . . .

References

QCD Phase Structure:

M. Alford, A. Schmitt, K. Rajagopal and T. Schäfer, Rev. Mod. Phys. 80 (2008) 1455.

D. Kharzeev, Proc. *The 18th Particles and Nuclei International Conference, PANIC08*, Eilat, Nucl. Phys. A 827 (2009) 118c.

L. McLerran, Proc. *The Sixth International Conference on the Physics and Astrophysics of Quark Gluon Plasma*, Goa, Nucl. Phys. A 862-863 (2011) 251.

S. Gupta, Proc. *The XXVIIIth International Symposium on Lattice Field Theory*, Villasimius, PoS (Lattice 2010) 007.

M.P. Lombardo, Proc. *The XXX International Symposium on Lattice Field Theory*, Cairns, PoS (Lattice 2012) 016.

S. Borsányi, Z. Fodor, S.D. Katz, S. Krieg, C. Ratti and K.K. Szabo, Phys. Rev. Lett. 111 (2013) 062005.

Flux Tube Description:

G. Ripka, *Dual Superconductor Models of Color Confinement*, Lecture Notes in Physics, Vol. 639, (Springer, Berlin, 2004).

A. Patel, Nucl. Phys. B 243 (1984) 411.

A. Patel, Phys. Lett. 139B (1984) 394.

A. Patel, Proc. *International Conference on the Physics and Astrophysics of Quark-Gluon Plasma*, Bombay, (World Scientific, Singapore, 1988), p.135.

A. Patel, Phys. Rev. D 85 (2012) 114019.

Lattice QCD Based Models:

J. Condella and C. DeTar, Phys. Rev. D 61 (2000) 074023.
M. Alford, S. Chandrasekharan, J. Cox and U.-J. Wiese, Nucl. Phys. B 602 (2001) 61.
S. Kim, P. de Forcrand, S. Kratochvila and T. Takaishi, Proc. *The XXIIIrd International Symposium on Lattice Field Theory*, Dublin, PoS (Lattice 2005) 166.
Y.D. Mercado, H.G. Evertz and C. Gattringer, Phys. Rev. Lett. 106 (2011) 222001.
P.N. Meisinger and M.C. Ogilvie, Phys. Lett. B 379 (2004) 163.
K. Fukushima, Phys. Lett. B 591 (2004) 277.
C. Ratti, M.A. Thaler and W. Weise, Phys. Rev. D 73 (2006) 014019.
M.C. Ogilvie, P.N. Meisinger and T.D. Wiser, Int. J. Theor. Phys. 50 (2011) 1042.
F. Karsch and K.-H. Mütter, Nucl. Phys. B 313 (1989) 541.
P. de Forcrand and M. Fromm, Phys. Rev. Lett. 104 (2010) 112005.

Experimental Data Analysis:

U.W. Heinz, Proc. *2nd CERN-CLAF School of High Energy Physics*, Mexico City, (2003) 165, `arXiv:hep-ph/0407360`.
B. Abelev *et al.* (STAR Collaboration), Phys. Rev. C 79 (2009) 034909.
C. Loizides, Proc. *23rd Rencontres de Blois, Particle Physics and Cosmology*, Blois, (2011).
L. Milano (ALICE Collaboration), Proc. *Quark Matter 2012*, Nucl. Phys. A 904-905 (2013) 531c.
S. Weinberg, *Cosmology*, (Oxford, New York, 2008).